

Validated thermodynamic prediction of AIP and eutectic (Si) solidification sequence in Al-Si cast alloys

S M Liang and R Schmid-Fetzer^a

Institute of Metallurgy, Clausthal University of Technology, D-38678 Clausthal-Zellerfeld, Germany

Email: ^aschmid-fetzer@tu-clausthal.de

Abstract. The eutectic microstructure in hypoeutectic Al-Si cast alloys is strongly influenced by AIP particles which are potent nuclei for the eutectic (Si) phase. The solidification sequence of AIP and (Si) phases is, thus, crucial for the nucleation of eutectic silicon with marked impact on its morphology. This study presents this interdependence between Si- and P-compositions, relevant for Al-Si cast alloys, on the solidification sequence of AIP and (Si). These data are predicted from a series of thermodynamic calculations. The predictions are based on a self-consistent thermodynamic description of the Al-Si-P ternary alloy system developed recently. They are validated by independent experimental studies on microstructure and undercooling in hypoeutectic Al-Si alloys. A constrained Scheil solidification simulation technique is applied to predict the undercooling under clean heterogeneous nucleation conditions, validated by dedicated experimental observations on entrained droplets. These specific undercooling values may be very large and their quantitative dependence on Si and P content of the Al alloy is presented.

1. Introduction

Chemical modification, with addition of Sr and/or Na, is a common process performed in Al-Si cast alloys to improve mechanical properties, especially tensile elongation. Trace additions of Sr (about a few hundred ppm) to hypoeutectic Al-Si alloys can result in a transformation of the eutectic silicon morphology from a coarse plate-like structure to a well refined fibrous structure [1-3]. However, the inhomogeneous modification with some coarse eutectic silicon can often be observed either in sand cast or permanent mould cast Al-Si alloys after Sr modification as shown in figure 1. A better understanding of the nucleation of Al-Si eutectic is essential for solving this problem. Many dedicated experimental studies have been carried out on the nucleation of Al-Si alloys, and it is generally accepted that the coarse eutectic Si nucleates on AIP particles [4, 5].

In our previous work [6], using a well developed thermodynamic description of the Al-Si-P ternary system, a precipitation map has been developed and the threshold value of P in Al-Si alloys has been determined. The calculated results not only agree with the microstructure and thermal analysis results of casting alloys but also with the dedicated entrained droplet experiments. In this work, we shall illustrate the careful comparison between the entrained droplet experimental and constrained Scheil simulation for Al-Si-P to facilitate understanding of the nucleation of eutectic Si.



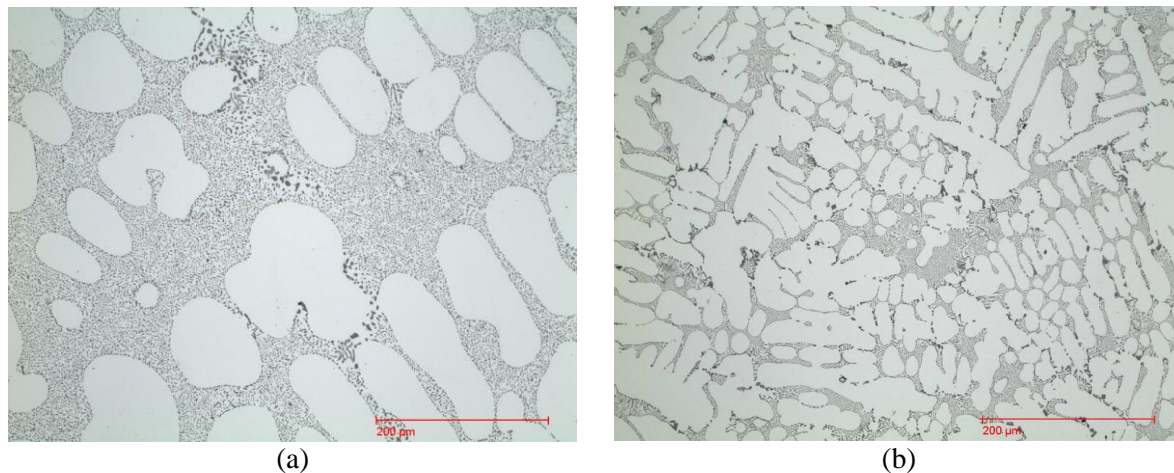


Figure 1. Inhomogeneous modification of Sr in Al-Si alloys (a) sand cast and (b) permanent mould cast.

2. Entrained droplet experiment and constrained Scheil simulation

Experimental studies of the nucleation of solidification are complicated by the presence of extraneous impurities. An entrained droplet technique, firstly developed by Wang and Smith [7], has proved successful in isolating extraneous impurities and thus achieving clean heterogeneous nucleation conditions. The entrained droplets technique includes two steps: Firstly, an alloy is rapidly solidified by melt spinning to produce a bimodal microstructure consisting of finely dispersed low melting second phase particles embedded in a higher melting point matrix. Subsequently, the alloy is carefully heated to just melt the second phase (droplets) while the matrix remains solid, and then slowly cooled in a thermal analyzer to solidify the entrained droplets. Extraneous impurities are segregated into an insignificant number of droplets, leaving clean nucleation conditions for a sufficiently large number of droplets entrained in the matrix. This technique has been successfully applied to Al-Si alloys [8-13].

A bimodal microstructure of Al-Si alloys can be obtained by melt spinning with some Al-Si eutectic droplets embedded in the Al matrix. The droplet solidification kinetics is studied by differential scanning calorimetry (DSC). The DSC spectrum of the cooling curve of the bimodal microstructure often presents two exothermic events. From the two exothermic onset temperatures, two eutectic nucleation temperatures, T_{N1} and T_{N2} , are determined. Then two values of eutectic nucleation undercooling, ΔT_1 and ΔT_2 , are defined as the difference between the Al-Si eutectic equilibrium temperature, 577 °C, and the experimentally observed T_{N1} and T_{N2} , respectively. The first peak refers to the solidification of the melt droplets located at grain boundaries normally with small undercooling, due to the large grain boundary fraction and enrichment of extraneous impurities. The second peak refers to the solidification of entrained droplets, in which the undercooling is largely associated with the nucleation ability of the heterogeneous nucleation sites under clean conditions.

The Scheil-Gulliver model [14], assuming equilibrium in the remaining liquid phase and blocked diffusion in the solidified solid phases, is often used as a simplified simulation of the solidification and phase formation of real cast alloys. During standard Scheil simulation, all phases are allowed to form without consideration of the nucleation barrier of different phases. The solid phase will immediately precipitate from the liquid provided its thermodynamic stability conditions are met. However, the formation of (Si) phase inside the entrained droplets of Al-Si alloys is largely constrained, due to lack of extraneous impurities for the heterogeneous nucleation of eutectic (Si) phase. An advanced "constrained Scheil" simulation is performed here to simulate the solidification of entrained droplets of Al-Si alloys. In constrained Scheil simulation the formation of (Si) phase is suspended based on the experimental fact that very large undercooling, well below the formation of (Si) under standard Scheil conditions, is observed. That is reflected in the constrained Scheil simulation by allowing the atoms of the droplet to distribute into any solid phase except (Si) under the local (metastable) equilibrium at the

liquid/solid interface. This simulation continues with growing undercooling below the stable eutectic (Si) temperature until the residual liquid composition in the droplet hits the saturation limit to precipitate another solid phase. In the present case this is AIP, which then triggers the immediate growth of (Si) at large undercooling, thus terminating the constrained Scheil simulation. Therefore, this constrained simulation is useful for the Al-Si-P alloys with P content below the threshold limit so that AIP does not form before the stable eutectic (Si). All thermodynamic calculations in the present work were performed using the integrated software package Pandat (www.computherm.com) [15] with the well developed thermodynamic description of Al-Si-P ternary system [6].

3. Comparison of calculated results with experimental data of Al-Si-P ternary alloys

Ho and Cantor [10] carried out a series of entrained droplets experiments for Al-3Si alloys with different levels of P. Three typical different levels of P are considered in this work for comparison with thermodynamic predictions, namely alloy 1: Al-3% Si-35ppm P; alloy 2: Al-3% Si-2ppm P and alloy 3: Al-3% Si-0.25ppm P. Mass% and ppm = $\mu\text{g/g}$ is used throughout this paper. These three levels of P in the Al-3Si alloys represent three types of solidification sequence, showing different morphology of eutectic Si and undercooling values. The ΔT_1 value is consistently observed at about 3 K in all alloys. This small undercooling is attributed to the droplets at grain boundaries with sufficient nucleation sites, also from impurities enriched in the eutectic melt at grain boundaries. However, the ΔT_2 value, corresponding to the eutectic nucleation in “clean” Al-Si-P droplets in the (Al) matrix, range from about 7–9 K to 60 K depending on the content of P. This dependency can be well explained by the constrained Scheil simulation.

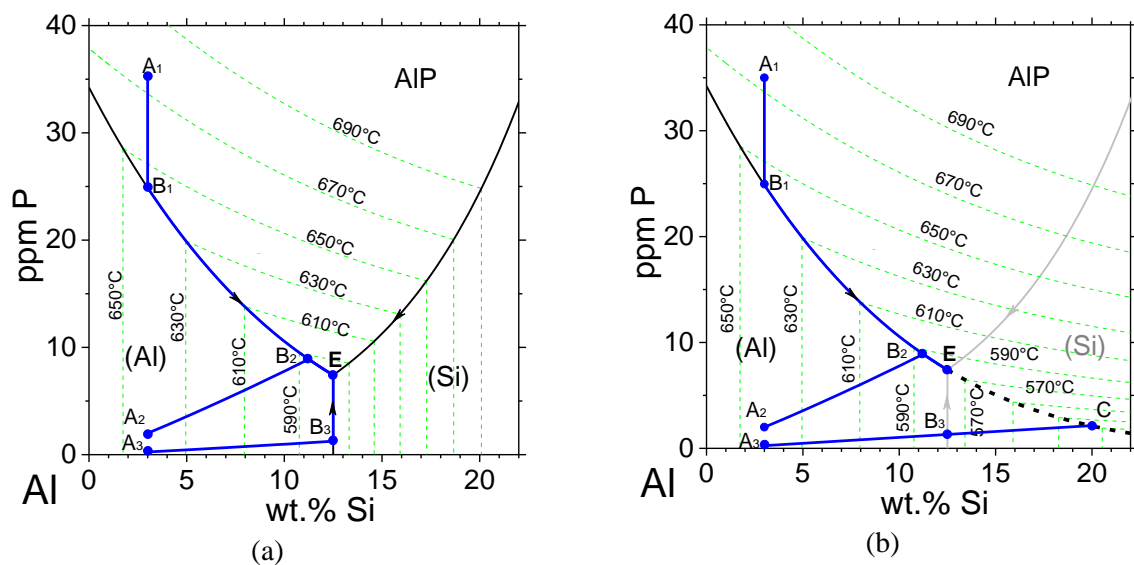


Figure 2. The solidification paths of the three alloys investigated in the work [10]: (a) standard Scheil solidification; (b) constrained Scheil solidification with suspended (Si) phase.

Figure 2(a) illustrates the liquidus projection of the Al-Si-P ternary system together with the standard Scheil solidification paths of the three alloys in [10]. All three alloys follow the solidification path of $A \rightarrow B \rightarrow E$ without considering the nucleation barrier of (Si) phases. Clearly, the solidification sequences of the alloys differ with P content increasing from 0.25 ppm P to 2 ppm P and 35 ppm P. The solidification path of alloy 1 (Al-3Si-35ppm P) is along $A_1 \rightarrow B_1 \rightarrow E$. The AIP phase is the primary phase precipitating before the (Al) phase, and the solidification sequence is $L \rightarrow \text{AIP} \rightarrow \text{AIP} + (\text{Al}) \rightarrow \text{AIP} + (\text{Al}) + (\text{Si})$. The solidification ends at ternary eutectic $L \rightarrow \text{AIP} + (\text{Al}) + (\text{Si})$. The solidification path of alloy 2 (Al-3Si-2ppm P) is along $A_2 \rightarrow B_2 \rightarrow E$, with solidification sequence

$L \rightarrow (Al) \rightarrow (Al) + AIP \rightarrow (Al) + AIP + (Si)$. The AIP phase precipitates after the (Al) phase but before the (Si) phase. The solidification of alloy 3 (Al-3Si-0.25ppm P) follows the path $A_3 \rightarrow B_3 \rightarrow E$, with solidification sequence $L \rightarrow (Al) \rightarrow (Al) + (Si) \rightarrow (Al) + (Si) + AIP$. The AIP phase can only form at the last stage of solidification at ternary eutectic $L \rightarrow AIP + (Al) + (Si)$ after the monovariant $L \rightarrow (Al) + (Si)$ eutectic.

If no effective potential nuclei are available in the melt for (Si) phase, then the formation of (Si) phase would be constrained. Figure 2(b) represents the solidification paths of the alloys under constrained Scheil simulation. In alloy 1 and alloy 2, the AIP phase precipitates before the start solidification of eutectic (Si), and can provide nucleation nuclei for eutectic (Si) phase. Therefore, solidification paths of alloy 1 and alloy 2 under the constrained Scheil simulation are the same as those under the standard Scheil simulation. On the other hand, for alloy 3, with 0.25 ppm P, no AIP precipitates before eutectic (Si) to facilitate the nucleation of Si, thus the formation of (Si) is suspended. The monovariant line $L \rightarrow (Al) + AIP$ will extend to lower temperature into the region of the suspended (Si). Thus, the solidification path under constrained Scheil simulation of alloy 3 is following $A_3 \rightarrow B_3 \rightarrow C$, rather than $A_3 \rightarrow B_3 \rightarrow E$. At point C, the melt is saturated with AIP which may now precipitate in the undercooled melt.

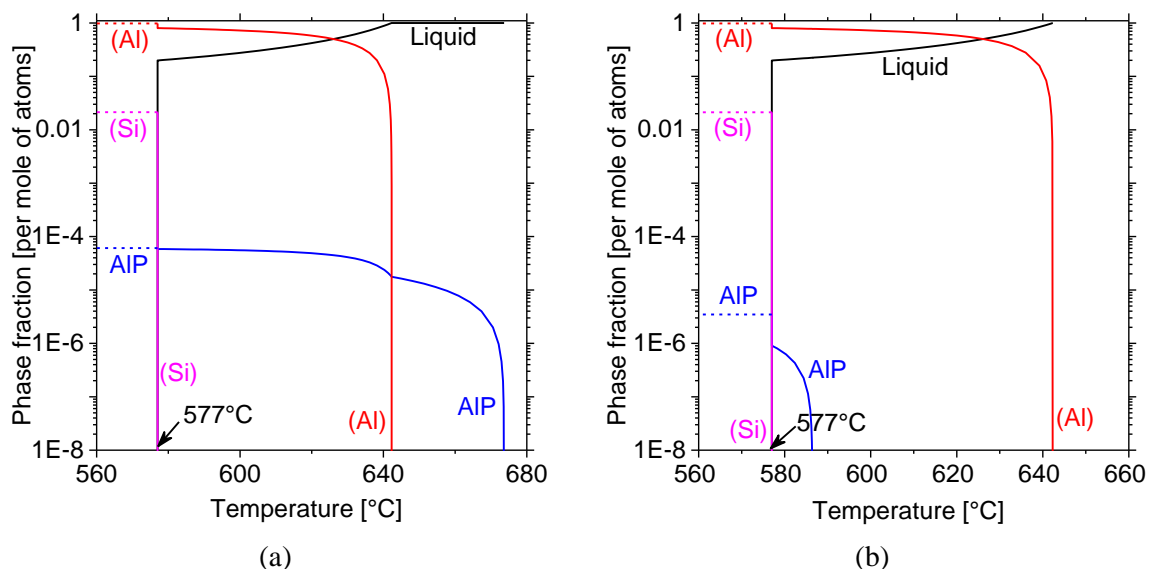


Figure 3. Phase fraction evolution of alloys during Scheil solidification simulation: (a) alloy 1: Al-3% Si-35 ppm P alloy; (b) alloy 2: Al-3% Si-2 ppm P alloy. The AIP phase precipitates before (Al) in Al-3% Si-35 ppm P alloy, and after (Al) but before eutectic (Si) in Al-3% Si-2 ppm P alloy.

Figure 3 represents the phase evolution of alloys 1 and 2 during the standard Scheil simulation, which is identical to the constrained Scheil simulation. The AIP phase precipitates before the (Si) phase and no undercooling of eutectic (Si) can be predicted in these two alloys, which is formally set to zero. The early precipitated AIP phase can provide effective nucleation sites for eutectic (Si), and generate coarse eutectic (Si) morphology. The DSC measured undercooling of alloy 1 and 2 are in the narrow range of 7–9 K, which is due to a kinetic nucleation effect that is beyond the scope of the thermodynamic treatment.

For alloy 3, the solidification sequence under standard Scheil simulation is $L \rightarrow (Al) \rightarrow (Al) + (Si) \rightarrow (Al) + (Si) + AIP$, shown by the solid lines in figure 4. In the constrained Scheil simulation the (Si) phase is suspended and solidification proceeds along the dashed lines in figure 4 until the formation of

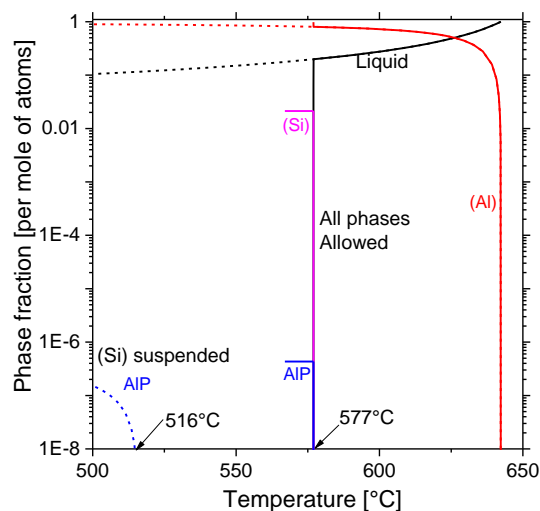


Figure 4. Scheil solidification simulation of alloy Al-3wt.% Si-0.25ppm P; the standard simulation (all phases are allowed to form, solid lines) is complemented by the constrained simulation, suspending the (Si) phase (dashed lines).

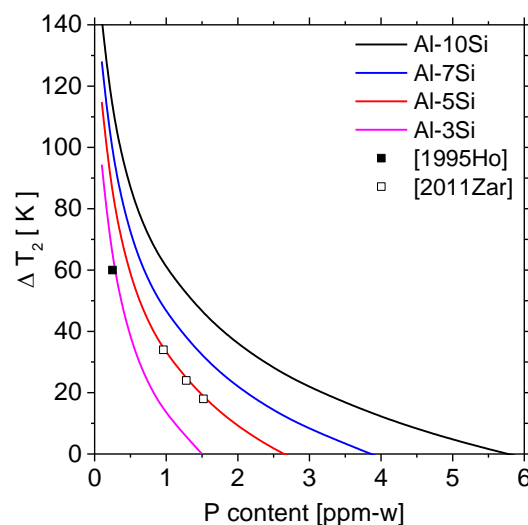


Figure 5. The interdependence of undercooling, ΔT_2 , and P content in Al-Si alloys predicted by constrained Scheil simulation. For the experimental data on Al-3Si [10] and Al-5Si alloys [12] the calculation was done as detailed in the text.

Table 1. Nucleation undercooling, ΔT_2 , of eutectic (Si) observed in entrained droplet experiments compared with the results predicted by the present thermodynamic calculation. Input values for the calculation are indicated by italic font and output values by bold font.

Alloy (wt.%)	P content (ppm)		ΔT_2 (K)		Exp. Ref
	Exp.	Calc. ^(a)	Exp.	Calc. ^(b)	
Al-5Si (HP)	< 2	1.0	34	34	[12]
Al-5Si (LP)	< 2	1.3	24	24	[12]
Al-5Si (HP) -P	< 2+0.5	1.5	18	18	[12]
Al-5Si (HP) -P	3	3	2	(0) ^(c)	[13]
Al-5Si (HP) -P	5	5	0	(0)	[13]
Al-3Si (UHP)	0.25	<i>0.25</i>	60	61	[10, 11]
Al-3Si (LP)	2	2	9	(0)	[10, 11]
Al-3Si (UHP) -P	35	35	7	(0)	[10, 11]
Al-3.58Si (UHP)	<1	0.3	63	63	[8]
Al-2.90Si (HP)	<1	0.5	37	37	[8]
Al-3.45Si (LP)	2	2	9	(0)	[8]

^(a) If a fixed experimental P content was reported it was applied as input value (italic font) for the calculation of ΔT_2 (bold font). If a range was reported the calculation was done inversely.

^(b) For the inverse calculation the experimental value of ΔT_2 (italic font) is used as input value and the P content (bold font) is calculated.

^(c) Zero (0) indicates that AIP forms before (Si) under normal Scheil conditions, therefore the constrained Scheil simulation cannot provide undercooling below the stable eutectic at 577°C. The P content is above the threshold value in these alloys.

AIP in the undercooled melt at 516 °C occurs. This AIP occurrence triggers the formation of eutectic (Si), thus, the predicted undercooling of (Si) is $\Delta T_2 = 61$ K. That value is shown in table 1 as calculated result, marked by bold font, where the given alloy composition used as input value for the calculation is marked by italic font. The analogous calculation (ΔT_2 obtained from given P content) results in the formal value of zero because the P content is above the threshold value and AIP forms before (Si) under normal Scheil conditions as detailed in figure 3. Indeed, a small value of ΔT_2 , not higher than 9 K, is experimentally observed. For the other five alloys in table 1 a larger uncertainty is reported for the P content and, therefore, the inverse calculation was performed, P content obtained from ΔT_2 . These calculated P contents not only agree reasonably well with the reported experimental range for the alloys. For example, Zarif et al. [12] report a range (upper limit) of the P content in their three Al-5Si alloys. The measured ΔT_2 values for their high purity (HP) — low purity (LP) — and P added alloys are 34, 24, and 18 K, respectively. The calculated P content shows a reasonable trend of 1.0 ppm — 1.3 ppm — 1.5 ppm. More importantly, as clearly stated by [12], the most accurate value is the difference of 0.5 ppm P added deliberately to the Al-5Si (HP) alloy to produce the Al-5Si (HP)-P alloy. The calculated difference is also 0.5 ppm P (exactly 0.56 ppm) and that indicates perfect agreement with the experimental observation. The same realistic trend is also shown for the ultra high purity (UHP) and HP alloys of [8] with calculated values of 0.3 and 0.5 ppm P, respectively. All entrained droplet results are collected in table 1, they all support the present thermodynamic approach. Based on this validated method the relationship between P content and the value of ΔT_2 is calculated for a range of Al-Si alloys with 3, 5, 7, and 10 % Si as shown in figure 5. It is noted that the determination of P content in Al alloys in the ppm range is difficult and associated with some error bar that also applies to the calculated values.

4. Conclusion

Normal and constrained Scheil simulation has been successfully applied to simulate the solidification of Al-Si-P alloys. For P content above a threshold value the solidification sequence switches so that AIP is formed before eutectic silicon, resulting in coarse eutectic morphology and small undercooling.

The P threshold value is strongly dependent on the Si content of hypoeutectic Al-Si alloys and may reach up to 7.4 ppm P for the eutectic Al-12.5Si alloy. The quantitative information on the P content is therefore important and the often provided purity information "below 10 ppm P" is insufficient.

For alloys with purity below the P threshold value very large undercooling may occur under clean nucleation conditions, such as found in entrained droplets. This undercooling, ΔT_2 , can be quantitatively predicted by the constrained Scheil simulation approach, indicating that the formation of (Si) may be suppressed until the metastable saturation with AIP is encountered, which subsequently triggers the formation of eutectic silicon on this potent nucleant. The value of ΔT_2 depends strongly on both the P and Si content of the alloy as demonstrated in figure 5.

References

- [1] Heusler L, Schneider W 1997 *AFS Transactions* **105** 915
- [2] Dahle A *et al.* 2001 *Metall. Mater. Trans. A* **32** 949
- [3] Cho Y H *et al.* 2008 *Metall. Mater. Trans. A* **39** 2435
- [4] Nogita K *et al.* 2004 *J. Electron Microsc.* **53** 361
- [5] Dahle A K *et al.* 2005 *Mater. Sci. Eng. A* **413-414** 243
- [6] Liang S-M, Schmid-Fetzer R 2014 *Acta Mater.* **72** 41
- [7] Wang C-C, Smith C S 1950 *AIME Trans.* **188** 136
- [8] Zhang D L, Cantor B 1993 *Metall. Trans. A* **24** 1195
- [9] Cantor B 1994 *Mater. Sci. Eng. A* **178** 225
- [10] Ho C R, Cantor B 1995 *Acta Metall. Mater.* **43** 3231
- [11] Ho C R, Cantor B 1995 *J. Mater. Sci.* **30** 1912
- [12] Zarif M *et al.* 2011 *Metall. Mater. Trans. A* **42** 1684
- [13] Li J H *et al.* 2014 *Acta Mater.* **72** 80

[14] Scheil E 1942 *Z. Metallkd.* **34** 70

[15] Cao W *et al.* 2009 *Calphad* **33** 328